CFD modelling of combustion in Heavy-Duty Diesel Engines

G. D'Errico°, T. Lucchini°, A. Onorati°
G. Hardy*,
° Department of Energy, Politecnico di Milano, Milano
* FPT Motorenforschung, Arbon

Keywords: Heavy-Duty Diesel Engines, OpenFOAM, Lib-ICE, flamelet, engine simulation

1 Abstract

The design and optimization stages of combustion systems for modern Heavy Duty Diesel engines must be supported by reliable CFD tools for the definition of the chamber geometry and injection strategy. To be fully predictive in terms of in-cylinder thermodynamics and flame structure, the employed combustion models must account for complex chemistry and turbulence-kinetics interactions. Within this context, the authors have implemented into an open-source code a model based on the multiple Representative Interactive Flamelets approach (*mRIF*) and applied it to Diesel combustion simulations. New numerical techniques were integrated in the proposed *mRIF* model in order to speed up the CPU time in integrating chemistry and the β-pdf of the chemical species to compute composition in the CFD domain. A parallel validation was performed both with constant-volume and Heavy-Duty Diesel Engine experiments, selecting similar operating conditions. In such way, both flame structure and heat release rate predictions are analyzed and the model capabilities with respect to its set-up and mesh structure are assessed.

2 Introduction

Development of heavy duty Diesel engines is strongly affected by more and more demanding requirements for a contemporary reduction of both fuel consumption and pollutant emissions. To fulfill such objectives, a combination and integration of different technologies is necessary: efficient combustion systems, engine downsizing, new after-treatment devices and heat recovery [7, 11, 8, 19]. In particular, fuel-air mixing and combustion processes must be investigated and optimized in detail since they both affect the quality of exhaust gases and energy conversion efficiency. Within this context, promising solutions appear to be the use of very high injection pressures (up to 3000 bar), further increase of full-load bmep, extension of engine operating range with advanced combustion

modes and dual fuel combustion. However, Diesel combustion is a very complex process involving many interacting physical phenomena including evolution of multi-phase flows, hydrocarbon auto-ignition and diffusion flame propagation in a inhomogeneous, turbulent high-pressure flow [4]. To this end, both advanced numerical and experimental tools are necessary for a detailed study of the combustion process. For what concerns numerical approaches, nowadays research is focused on the development of models based on complex chemistry and including turbulence-kinetics interactions for a proper prediction of auto-ignition, flame structure evolution, soot and NO_x emissions formation.

Most of the models which are used for combustion simulations with detailed chemistry are based on flame structure assumptions (equivalent stretched diffusion flame, partially-stirred reactor, homogeneous reactor, ...) and compute chemical composition or reaction rate in each computational cell accordingly [9, 24]. Among the available approaches, both Representative Interactive Flamelets (RIF) and zero-dimensional Conditional Moment Closure (CMC) operate a coordinate transformation that makes possible to solve the diffusion-reaction problem in the mixture fraction space, that is considered to be the predominant variable in non-premixed combustion problems [2, 27]. The effects of local flow are incorporated in the scalar dissipation rate variable and chemical composition is estimated by assuming a presumed statistical distribution of each chemical species that depends on mixture fraction and its variance. Since most of the development efforts for Heavy Duty Diesel Engine Combustion are focused to full-load conditions (where a large amount of fuel is injected at very high pressures), both heat transfer and flame-wall interaction processes need also to be properly taken into account.

This work presents a methodology for combustion and pollutant emissions prediction in Heavy-Duty Diesel engines, based on the application of a Multiple Representative Interactive flamelet model (*mRIF*) which was successfully applied in past works [5, 6] for simulations at constant-volume conditions. The *mRIF* model approximates the flame structure as a set of multiple unsteady laminar diffusion flames (*flamelets*) and their evolution is computed in the mixture fraction space [2] where species and energy equations are solved. The effects of mixing are incorporated in the scalar dissipation rate, which is calculated as a conditional average of its distribution in the CFD domain. The use of multiple flamelets ensures a better prediction of both flame structure and auto-ignition, since spatial variations of the scalar dissipation rate are properly taken into account [12, 2]. The *mRIF* model allows realistic simulations of Diesel with detailed chemistry, but incorporating large mechanisms in it (more than 50 species) drastically increases the computational time. In particular, the need to integrate the PDF for any chemical species in all the cells of the CFD domain introduces significant computational overheads. To this end, in this work two new techniques were developed to reduce the CPU time when the *mRIF* model is applied to IC engine combustion simulations. The first one is represented by the so-called *virtual species* approach, where a limited set of chemical species is used in the CFD domain to represent the entire set of the flamelet species. In this way, the PDF is integrated for a very limited number of chemical species but it is possible to adopt very large mechanisms. To further reduce the computational time, the PDF integration in the mixture fraction space is performed for clusters of cells having similar values of mixture fraction and variance. Finally, the TDAC algorithm was integrated into the *mRIF*

model, ensuring a significant reduction of CPU time when detailed chemistry is used, since it combines on-line techniques for reduction of chemical mechanism and reaction rates tabulation [3]. In this way, the ODE solver operates only on a limited number of computational cells for each time-step, with a reduced set of species and reactions.

The proposed approaches for combustion modeling were implemented in the Lib-ICE code, where the *mRIF* model was recently developed and validated [5, 6]. Lib-ICE is based on the OpenFOAM technology (`www.openfoam.org`) and includes a set of well validated spray sub-models to properly describe fuel atomization, secondary breakup and evaporation [15, 17]. Validation was performed into different steps. First, a set of operating conditions which are critical in terms of fuel consumption and emissions for a heavy duty diesel engine were identified. Then, the methodology was assessed at constant-volume conditions, simulating reacting and non-reacting cases with ambient temperature and pressure which are similar to those found at start of injection time in the studied engine. Computed data of ignition delay and flame lift-off were compared with experimental ones and the flame structure was analyzed to understand the capabilities of the model to properly describe propagation and stabilization of a turbulent diffusion flame. Finally, engine simulations were carried out for the three selected operating points. Validation at engine conditions was performed by comparing computed and experimental data of in-cylinder pressure, and heat-release rate.

3 Computational models

3.1 Multiple representative interactive flamelets (MRIF)

This model is based on the laminar flamelet concept, assuming that the smallest turbulent time and length scales are much larger than the chemical ones and there exists a locally undisturbed sheet where reactions occur [2]. This sheet can be treated as an ensemble of stretched counter-flow diffusion flames, called *flamelets*. The advantage of such treatment is that all reacting scalars only depend on the mixture fraction variable, Z, which is related to the local fuel-to-air ratio for non-premixed combustion. Hence, local chemical composition can be estimated from the Z field in the CFD domain, assuming that its sub-grid distribution can be represented by a β-pdf. To this end, transport equations for both Z and its variance $\widetilde{Z''^2}$ need to be solved:

$$\frac{\partial \rho \tilde{Z}}{\partial t} + \nabla \left(\rho \mathbf{U} Z \right) - \nabla \cdot \left(\frac{\mu_t}{Sc_Z} \nabla \tilde{Z} \right) = \dot{S} \tag{1}$$

$$\frac{\partial \rho \widetilde{Z''^2}}{\partial t} + \nabla \left(\rho \mathbf{U} \widetilde{Z''^2} \right) - \nabla \cdot \left(\frac{\mu_t}{Sc_{\widetilde{Z''^2}}} \nabla \widetilde{Z''^2} \right) = 2 \frac{\mu_t}{Sc_{\widetilde{Z''^2}}} \left| \nabla Z \right|^2 - \rho \chi$$

The sink term appearing in Eq. 2 is the average scalar dissipation rate, which is function of the turbulent time scale and mixture fraction variance:

$$\chi = C_\chi \frac{\varepsilon}{k} \widetilde{Z''^2} \tag{2}$$

where the constant C_χ was set to 2 in this work. In order to properly account for local flow and turbulence effects on the flame structure and predict flame stabilization, a multiple number of flamelets was used. Each one is representative of a certain portion of the injected fuel mass, and chemical composition in each cell is computed from mixture fraction and flamelet marker distribution as follows:

$$Y_i\left(\vec{x}\right) = \sum_{j=1}^{N_f} M_j \int_0^1 Y_{j,i}\left(Z\right) P\left(Z, \widetilde{Z''^2}\right) dZ \tag{3}$$

For each flamelet marker, the following transport equation is solved:

$$\frac{\partial \rho \tilde{M}_j}{\partial t} + \nabla\left(\rho \mathbf{U} \tilde{M}_j\right) - \nabla \cdot \left(\frac{\mu_t}{Sc_Z} \nabla \tilde{M}_j\right) = \dot{S}_{M_j} \tag{4}$$

where the source term $\dot{S}_{M_j}$ corresponds to $\dot{S}$ only for a specified interval of the injection duration, while it is zero elsewhere. Flamelet markers must also satisfy the following relation:

$$Z = \sum_{j=1}^{N_f} M_j \tag{5}$$

The local flame structure is defined by the flamelet equations that are solved assuming unity Lewis number [2] in the mixture fraction space:

$$\rho \frac{\partial Y_i}{\partial t} = \rho \frac{\chi_z}{2} \frac{\partial^2 Y_i}{\partial Z^2} + \dot{\omega}_i \tag{6}$$

$$\rho \frac{\partial h_s}{\partial t} = \rho \frac{\chi_z}{2} \frac{\partial^2 h_s}{\partial Z^2} + \dot{q}_s \tag{7}$$

where Y_i is the mass fraction of the species i, ρ is the density, Z the mixture fraction, $\dot{\omega}_i$ is the chemical source term of species i, h_s the sensible enthalpy and $\dot{q}_s$ the heat released by the chemical reactions. Eqns. 6 - 7 are solved on a 1-D mesh with the finite volume method, by employing an ODE stiff solver to properly compute $\dot{\omega}_i$. Effects of mixing related to turbulence and flow-field are grouped into the scalar dissipation rate term χ_z expressed as:

$$\chi_z = \widehat{\chi_{st,j}} \frac{f\left(Z\right)}{f\left(Z_{st}\right)} \tag{8}$$

$f\left(Z\right)$ has an erfc-profile [21], while scalar dissipation rate at stoichiometric mixture fraction conditions $\widehat{\chi_{st,i}}$ for each flamelet is computed as an average of the local values in each computational cell:

$$\widehat{\chi_{st,j}} = \frac{\int_V M_j \chi_{st,l}^{3/2} \rho \tilde{P}\left(Z_{st}\right) dV'}{\int_V M_j \chi_{st,l}^{1/2} \rho \tilde{P}\left(Z_{st}\right) dV'} \tag{9}$$

where P is a β-function, whose parameters depend on mixture fraction and its variance. In each cell $\chi_{st,l}$ is computed following the Hellstrom formulation [2]:

$$\chi_{st,l} = \frac{\chi}{\int_0^1 \frac{f(Z)}{f(Z_{st})} \tilde{P}\left(Z\right) dZ} \tag{10}$$

Fig. 1 summarizes the operation of the *mRIF* combustion model, illustrating the mutual interactions between the CFD and flamelets domains. At each time-step, average stoichiometric scalar dissipation rate values are passed to each flamelet, that solves Eqn. 6-7 accordingly. The chemical composition in the CFD domain is computed from the mixture fraction, its variance and the flamelet marker distribution. Temperature is updated from new chemical composition and total enthalpy, whose variation is only due to flow and spray evaporation. For further information, the reader is referred to [12].

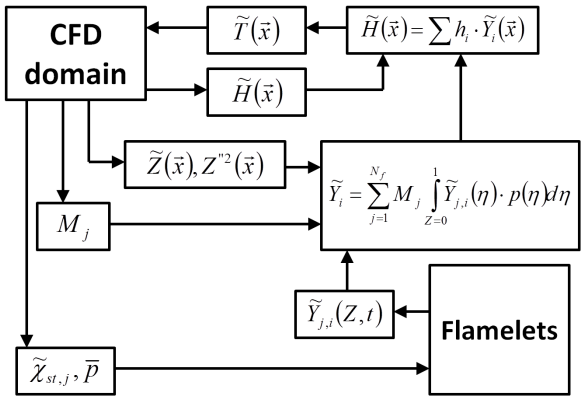

Figure 1: Operation of *mRIF* model: interaction between flamelets and CFD domain

3.2 Reduction of computational time

One of the advantages of the *mRIF* model compared to other ones based on detailed chemistry is represented by the fact that the reaction-diffusion problem is solved in the mixture fraction space, which is approximated as a one-dimensional grid with a limited number of points (100-200). This drastically reduces the CPU time required for chemistry integration and makes possible to use large mechanisms (more than 100 species) with a better prediction of both combustion and pollutant emissions. However, mechanisms with many species introduce very high computational overheads since:

1. When increasing the number of flamelets, the time spent in chemistry integration for all of them becomes very high and, again, limits the maximum number of species that can be used;

2. Integration of the PDF of the chemical species to compute composition in the computational domain, according to Eq. 3, requires a significant amount of time. Being N_c the number of cells in the CFD mesh, N_z the number of points in the mixture fraction domain, N_f the total number of flamelets and N_s the chemical species in the mechanism, the number of operations needed is approximately $N_c \times N_z \times N_f \times N_s$ which is of the order of 10^{10} in case of $N_c = 3 \cdot 10^4$, $N_z = 200$, $N_f = 50$ and $N_s = 100$.

To reduce the CPU time required by the *mRIF* combustion model and make it suitable for practical calculations efforts were focused towards the development

of efficient solutions both for integration of the β-pdf and to handle detailed chemistry in the flamelet domain. For what concerns point 1, the TDAC algorithm was employed to drastically reduce the CPU time required by the ODE stiff solver to compute reaction rates for each chemical species. To address point 2, two new approaches were developed named *virtual species* and *cell clustering*, respectively.

3.2.1 Tabulation of dynamic adaptive chemistry (TDAC)

When detailed chemistry is incorporated in combustion models, it is necessary to consider that chemical time-scales are much smaller (2-4 orders of magnitude) than the CFD time-step which is generally used ($10^{-7} - 10^{-5}$). For this reason, ODE stiff solvers need to be employed to properly compute the chemical species reaction rates that are used in the chemical species transport equations, as shown in Eqns. 6. However, operation of ODE solvers significantly increase the computational time since it involves sub-cycling and computations of large jacobians. Hence, the sizes of mechanisms employed in practical simulations are generally limited to 50 species and 100 reactions [20, 14] with a consequent lack in terms of accuracy mainly when advanced combustion modes, high EGR conditions and soot formation processes need to be computed. To make the use of more detailed mechanisms possible (up to 150 species for Diesel combustion) in a reasonable amount of time, the TDAC algorithm [3] was employed in this work that combines the ISAT and DAC techniques [25, 13].

The ISAT algorithm intends to reuse computationally demanding results, e.g. the integration of large and stiff ODE systems, by storing those results and all the necessary data to retrieve them. During computation, given a query point, ψ^q, it computes a linear approximation of the mapping:

$$\mathbf{R}(\psi^q) \approx \mathbf{R}^l(\psi^q) = \mathbf{R}(\psi^0) + \delta\mathbf{R}^l \ , \tag{11}$$

where $\delta\mathbf{R}^l = \mathbf{A}(\psi^0)(\psi^q - \psi^0)$ and $\mathbf{A}$ is the mapping gradient matrix defined by

$$A_{ij}(\psi^0) = \frac{\partial R_i(\psi^0)}{\partial \psi_j} \ . \tag{12}$$

The linear approximation defined by equation (11) is valid in the region of accuracy (ROA) where the following condition is respected:

$$|\mathbf{R}(\psi^q) - \mathbf{R}^l(\psi^q)| = |\delta\mathbf{R} - \delta\mathbf{R}^l| \leq \varepsilon_{\text{ISAT}} \ , \tag{13}$$

where $\varepsilon_{\text{ISAT}}$ is a user-specified tolerance and $\delta\mathbf{R} = \mathbf{R}(\psi^q) - \mathbf{R}(\psi^0)$. During the calculation, the table is built up according to the received queries. It consists of a binary tree with leafs and nodes. The leafs store ψ, $\mathbf{R}(\psi)$, $\mathbf{A}(\psi)$ and the ROA description. The nodes contain the rules that allow to scan the binary tree to retrieve the appropriate point [25].

The DAC method computes reduced mechanisms that are valid for the local thermo-chemical conditions. In this work, DAC has been extended to full CFD meshes with wall heat transfer. The reduction algorithm is executed before every call to the stiff solver according to the directed relation graph (DRG) method, which identifies the relevant species and reactions according to the thermodynamic conditions in each cell [13].

The coupling of ISAT and DAC performed in this work is schematically illustrated in Figure 2. When ISAT receives a query ψ^q that needs to integrate the ODE set, it provides ψ^q to the DAC algorithm which then finds the reduced mechanism for the local thermo-chemical conditions and provides the reduced set of active species ψ_a^q to the ODE solver. This solver computes the reaction mapping for the reduced set $\mathrm{R}(\psi_a^q)$ that is used by ISAT to build the reaction mapping $\mathrm{R}(\psi^q)$ in the full composition space. Using simplification methods at distinct levels combines their effects and allows a significant reduction of the computational cost. The use of TDAC ensures speed-up factors ranging from 10 to 1000 depending on the mechanism size and simulated combustion mode [3].

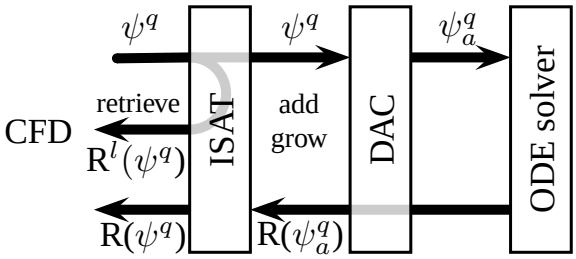

Figure 2: TDAC: combination of ISAT and DAC

3.2.2 The virtual species approach

To properly employ detailed chemistry for the *mRIF* combustion model but, at the same time, avoid accounting in the geometry domain for all the species included in the chemical mechanism, the *virtual species* approach was developed in this work. A reduced set of chemical species $Y_{v,i}\left(\mathbf{x}\right)$ is considered in the CFD mesh and composition of $Y_{v,i}\left(Z\right)$ in the mixture fraction space is computed to consistently preserve both mass and thermodynamic properties of the entire set of chemical species used in each flamelet. In this way, the β-pdf is integrated only for $Y_{v,i}$ in a limited amount of CPU time. In particular, seven chemical species were used in this work (N_2, O_2, $fuel$, CO_2, CO, H_2O, H_2) and their composition in the mixture fraction space $Y_{v,i}\left(Z\right)$ is computed for any flamelet j as follows:

- For very rich mixtures ($\phi > 4$), where six virtual species are considered (N_2, $fuel$, CO_2, CO, H_2O, H_2):

$$\sigma_H\left(Z\right)_j = \sum_{i=1}^{N_s} N_{H,i} \cdot x_i\left(Z\right)_j = \sum_{k=1}^{N_v} N_{H,k} \cdot x_{v,i}\left(Z\right)_j \tag{14}$$

$$\sigma_C\left(Z\right)_j = \sum_{i=1}^{N_s} N_{C,i} \cdot x_i\left(Z\right)_j = \sum_{k=1}^{N_v} N_{C,k} \cdot x_{v,i}\left(Z\right)_j \tag{15}$$

$$\sigma_O\left(Z\right)_j = \sum_{i=1}^{N_s} N_{O,i} \cdot x_i\left(Z\right)_j = \sum_{k=1}^{N_v} N_{C,k} \cdot x_{v,i}\left(Z\right)_j \tag{16}$$

$$\sigma_N\left(Z\right)_j = \sum_{i=1}^{N_s} N_{N,i} \cdot x_i\left(Z\right)_j = \sum_{k=1}^{N_v} N_{N,k} \cdot x_{v,i}\left(Z\right)_j \tag{17}$$

$$h\left(Z\right)_j = \sum_{i=1}^{N_s} Y_i\left(Z\right)_j h_i\left(T\big(Z\big)_j\right) = \sum_{k=1}^{N_v} Y_{i,v}\big(Z\big) h_i\big(T\left(Z\right)\big) \tag{18}$$

- In case of lean, stoichiometric or rich mixtures ($\phi \leq 4$), seven virtual species are taken into account (O_2 is added to the set) and an additional equation is solved to preserve also the mass specific heat:

$$c_p\left(Z\right)_j = \sum_{i=1}^{N_s} Y_i\left(Z\right)_j c_{p,i}\big(T\left(Z\right)_j\big) = \sum_{k=1}^{N_v} Y_{i,v}\left(Z\right)_j c_{p,k}\big(T\left(Z\right)_j\big) \tag{19}$$

In Eqns. 14-19, σ is the total number of elements (C, H, O and N) in each flamelet for a mixture fraction value Z; N_s is the total number of species in the flamelet domain; N_v is the total number of virtual species (six or seven); N is the total number of elements (C, H, O and N) in each chemical species; x refers to mole fractions; Y refers to mass fractions; h is the mass specific enthalpy (sensible + formation); c_p is the mass specific heat.

3.2.3 Cell clustering for β-pdf integration

The *virtual species* approach reduces the number of chemical species for which integration of the β-pdf is necessary. However, such step still remains time-consuming when many flamelets (> 20) and fine meshes (30000 - 100000 cells) are used as it happens in engine simulations. Furthermore, due to the axy-symmetrical nature of the Diesel spray, it is expected that many cells will have very similar values of both mixture fraction and variance. For this reason, using the same chemical composition computed from the flamelet domain for groups of cells with similar Z and $\widetilde{Z''^2}$ is expected to save a large amount of time without compromising the accuracy of the computed results. Such approach was followed in this work: cells are grouped into Z-$\widetilde{Z''^2}$ zones according to user-specified parameters, then the β-pdf integration is performed for each zone and computed chemical composition is mapped back from zones to the corresponding CFD cells. At each time-step, cells are clustered into zones according to:

- Minimum and maximum values of mixture fraction and variance in the CFD domain;

- Discretization parameters for the creation of the Z-Z''^2 space, specified by the user.

A schematic of the cell clustering algorithm developed for the β-PDF integration is illustrated in Fig. 3.

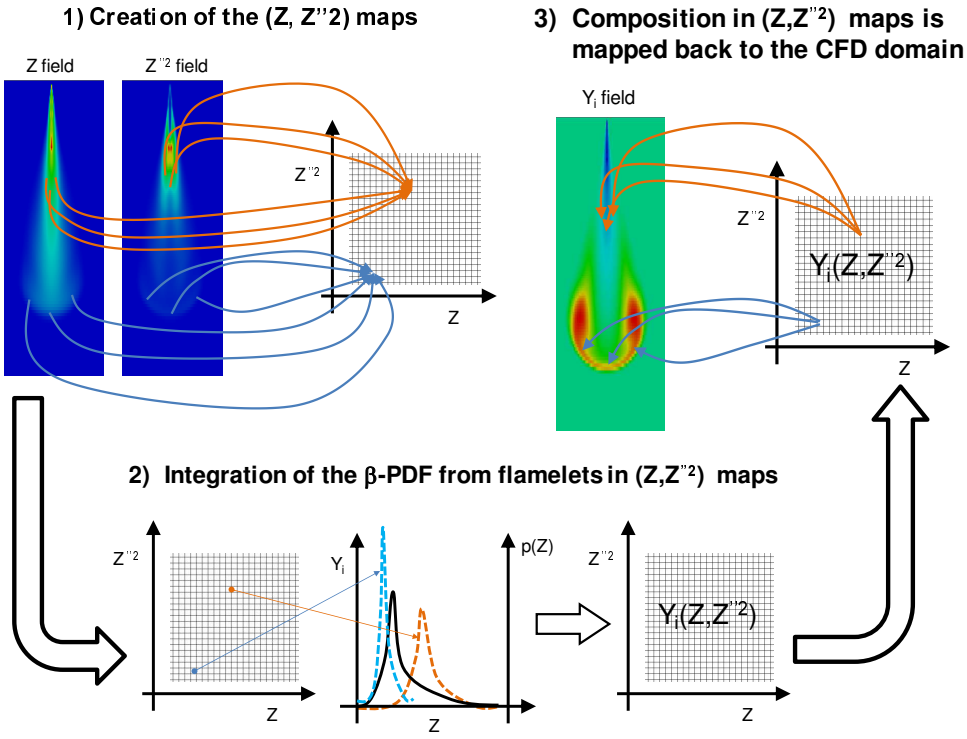

Figure 3: Cell clustering algorithm developed for the β-PDF integration. Step 1: Creation of the Z-$Z^{''2}$ according to user specified parameters; Step 2: Integration of the β-PDF from flamelets in the Z-$Z^{''2}$ maps; Step 3: Composition in Z-$Z^{''2}$ maps mapped back to the CFD domain.

4 Experimental validation

4.1 Heavy Duty engine data

Experiments carried out for a heavy-duty, Euro 6 Diesel engine were used to validate the proposed approach for combustion modeling. The main engine data are summarized in Table 1. The Common-Rail injection system operates at a maximum pressure of 1600 bar and delivers fuel to the six cylinders through 8-hole nozzle injectors.

Validation of the proposed CFD methodology was performed using three operating points displayed in Fig. 4 with each one of them being of relevance for operation, design and optimization of heavy-duty diesel engines. In particular, operating point 1 represents full-torque conditions, where a large amount of fuel is injected and interaction between flame and wall is expected to influence significantly the combustion process. Fuel consumption is minimum in operating point 2, while in the middle-load condition (operating point 3) soot emissions need to be controlled. For both such operating points a double injection strategy (pilot + main) was used. Further details about the simulated conditions are provided in Table 2. Finally, Table 3 summarizes the in-cylinder estimated thermodynamic conditions which are found at SOI time for the three selected

operating points.

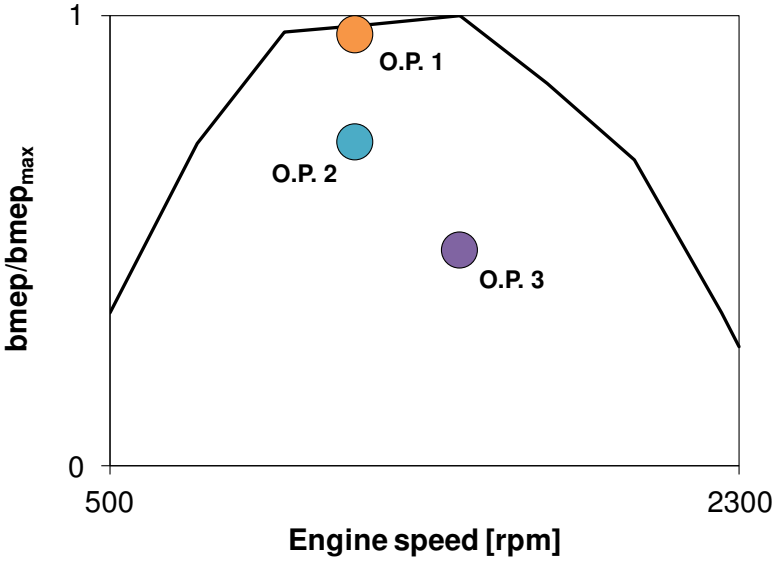

Figure 4: Simulated engine operating points.

4.2 Validation at constant-volume conditions

For a proper prediction of the combustion process at different engine loads and accounting for injection pressure variations, reliable numerical tools are necessary to estimate how such engine parameters affect liquid spray evolution, air/fuel mixing process, ignition delay and flame propagation. To this end, a preliminary validation was carried out at constant-volume conditions, simulating n-dodecane spray combustion in the so-called *Spray-A* experiment carried out in the Sandia Combustion Vessel, whose data are publicly available within the context of the Engine Combustion Network database [18, 22]. Fuel is de-

Table 1: Main data of the simulated engine

Cylinders	6
Bore	128 mm
Stroke	144 mm
Compression ratio	16.5
Swirl ratio	1.4
Injection system	Common-Rail
Maximum injection pressure	1600 bar
Hole number	8
Nozzle hole diameter	0.2 mm
Air management	VGT turbocharger + wastegate

Table 2: Details of the simulated operating points

Operating point	Speed [rpm]	Load [%]	λ [-]	EGR [%]	Injection strategy	Injection pressure [bar]
1	1200	100	1.5	0	Only main	750
2	1200	75	1.8	0	Pilot + main	750
3	1500	50	2.1	0	Pilot + main	1100

Table 3: Details of the simulated operating points

Operating point	Pressure [bar]	Temperature [K]	density [kg/m^3]
1	103	943	38
2	99	943	37
3	82	952	30

livered through a single-hole, 90 μm nozzle at pressures ranging between 500 and 1500 bar. Calculations were carried out in a 2D, axy-symmetric mesh with grading: it has a minimum mesh size of 0.1 mm and a successive growth ratio of 1.01. The grid represent a 1/72 portion of the combustion chamber, with a 108 mm height and 54 mm width; it has 216 cells in the axial direction and 108 in the radial one. Oxidation process of n-dodecane is described by means of a skeletal detailed reaction mechanism with 106 species and 420 reactions [26]. Its size can be considered acceptable for CFD computations of diesel spray combustion both at constant-volume and in engine geometries. operating points were considered for what concerns constant volume conditions, and they are summarized in Table 4. Initially, non-reacting conditions (operating point SA1) were considered to properly assess and validate the spray model. Then, effect of injection pressure on combustion process was evaluated (points SA2, SA3, SA4), following variation of engine speed for the considered engine. Purpose of points SA5 and SA6 is to verify if the adopted kinetic mechanism is able to reproduce ignition delays at ambient oxygen conditions and densities similar to those found in the studied diesel engine. Despite some important differences between engine and Sandia vessel experiments exist mainly in terms of injector sizes, there are also important similarities for what concerns injection pressure and ambient conditions. Hence, validation of the proposed model for the spray-A experiment represent a first important step towards its application to combustion simulations in heavy-duty engines.

Non reacting conditions were first simulated, to properly assess the spray sub-models. Here, the KHRT model by Reitz et al. [23] was used to predict both primary and secondary atomization. The standard $k-\varepsilon$ model was used for turbulence with the C_1 constant modified to 1.55 as it is commonly done to predict penetration and diffusion of jets. Validation of the spray model is illustrated in Figs. 5(a)-(b) for the non-reacting condition (T = 900 K, ρ = 22.8 kg/m^3). Fig. 5(a) compares computed and experimental data of liquid and vapor penetra-

Table 4: Details of the simulated operating points

Operating point	Temperature [K]	Density [kg/m^3]	p_{inj} [bar]	O_2 [% by vol.]	Δt_{inj} ms
SA1	900	22.8	150	0	4
SA2	900	22.8	150	15	4
SA3	900	22.8	100	15	4
SA4	900	22.8	50	15	4
SA5	900	22.8	150	21	4
SA6	900	30	150	21	4

tion for different instants after start of injection (ASOI). In Fig. 5(b), computed distribution of mixture fraction is compared with post-processed and averaged experimental data that were obtained by means of the Raleigh-scattering technique [10]. The model properly reproduces the experimental trends in terms of liquid and vapor penetration. Furthermore, distribution of mixture fraction is rather well predicted in the entire domain and this is a very important prerequisite for the validation of any combustion model.

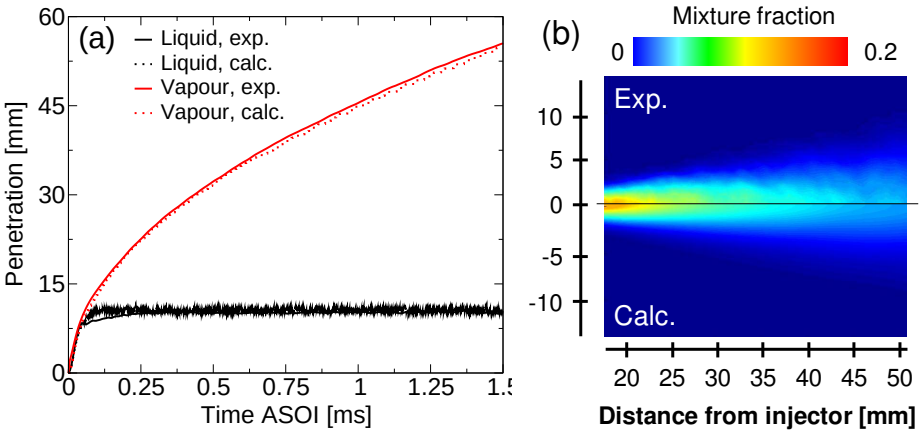

Figure 5: (a): Spray model assessment and validation: comparison between computed and experimental data of fuel liquid and vapor penetrations; (b): Comparison between computed and experimental distributions on a symmetry plane at 4 ms after start of injection. Ambient conditions: $\rho = 22.8 kg/m^3; T = 900K$

Once the spray model was properly assessed, combustion simulations were carried out for the remainder of the operating points listed in Table 3. For what concerns the *mRIF* setup, every 0.1 ms from the start of injection a new flamelet was introduced and initialized with the solution taken from the previous one both in terms of temperature and chemical species distribution in the mixture fraction domain. Figs. 6(a)-(b) reports a comparison between computed and experimental ignition delays: numerically ignition delay was defined as the time from the start of injection to the time where the maximum rate of

maximum temperature rise happens, while the lift-off length (LOL) was defined as the distance from the injector to the axial position of 2% of its steady-state OH mass fraction. These definitions were both suggested from the Engine Combustion Network. In Fig. 6(a) it is possible to see that the proposed combustion model follows rather well the experimental trend in terms of ignition delay time. In particular, with respect to the baseline case (SA2), a reduction of injection pressure slightly increase the ignition delay time (SA3 and SA4). For what concerns case SA5, the increase of oxygen concentration (21% compared to 15% by volume) is responsible for the reduction of ignition delay. No experimental data were available for SA6 conditions, with the highest density, however the ignition delay reduction compared to the baseline condition seems to be reasonable and mainly related to the highest chemical species reaction rates due to the higher ambient density. Despite ignition delay data are estimated rather well, there is a slight overestimation for any case of approximately 0.15 ms which can be mainly ascribed to the kinetic mechanism used.

A proper prediction of the flame stabilization process seems to be very important for a proper estimation of soot formation and heat release, as discussed in [10]. In past works [5, 6] authors illustrated that, for the *mRIF* model, the mechanism governing flame-lift off is represented by the auto-ignition of a diffusion flame. In particular, flamelets evolving in the CFD domain initially experience very high scalar dissipation rate values above the extinction limit χ_{ig} and no chemical reaction occurs. As soon as the scalar dissipation rate goes below χ_{ig} chemical reactions start to occur and ignition for each flamelet is mainly affected by mixture fraction distribution, ambient conditions and fuel chemistry. However, estimation of the scalar dissipation rate requires a very accurate description of the fuel-air mixing process with a very fine mesh near the nozzle. Use of coarse grids or not properly accounting for the axy-symmetry of the spray will lead to underestimation of the scalar dissipation rate and, consequently, to non-correct prediction of the lift-off length. Here lift-off lengths are rather well-predicted for all the analyzed conditions. In particular, effect of injection pressure seems to be properly reproduced by the *mRIF* model.

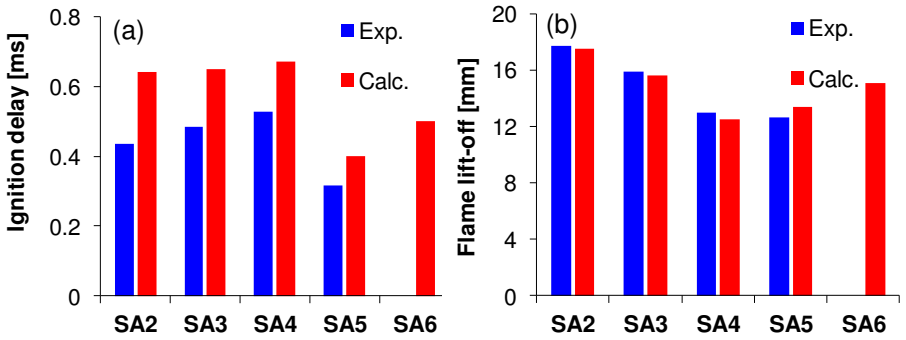

Figure 6: (a): Comparison between computed and experimental data of ignition delay for the selected reacting operating conditions; (b):Comparison between computed and experimental data of lift-off length for the selected reacting operating conditions.

Reduction of injection pressure seems to have two opposite effects: increase

of ignition delay and, at the same time, reduction of flame lift-off length. Ignition delay time is mainly affected by the evolution of the scalar dissipation rate for the first flamelets. In particular, Figs. 7(a)-(b) displays, at 0.2 and 0.6 ms after SOI the distribution of the scalar dissipation rate for the three different injection pressures considered. On the same figure, the stoichiometric mixture fraction iso-contour is also shown with white line. Few instants after start of injection (0.2 ms ASOI), Fig. 7(a), it is possible to see that reduced vapor penetration is responsible for higher scalar dissipation rate values in the stoichiometric region for the low injection pressure case. Later during injection (0.6 ms ASOI), distribution of scalar dissipation rate in the computational domain changes and, in particular, for the highest injection pressure it is possible to see that there is a large region where scalar dissipation rate remains higher. For this reason, ignition of the first flamelets will be faster for the cases with high injection pressure, but next ones will find higher scalar dissipation rate values and they will require more time to be ignited. Since auto-ignition of a diffusion flame is the stabilization mechanism for the *mRIF* model, higher injection pressures will lead to increased lift-off lengths.

4.3 Engine simulations

Once the proposed approach was assessed and properly validated at constant-volume conditions, simulations of the combustion process were carried out in the heavy duty engine for the three selected operating points listed in Table 2. A 1/8 sector of the combustion chamber was simulated, and details of the computational mesh are displayed in Fig. 8. Additional compensation volumes were included either in the head and in the crevices parts to properly fit the experimental compression ratio. To keep the mesh resolution as much constant as possible in the radial direction, two prismatic layers of cells were inserted to increase the number of cells when moving far from the nozzle. To improve prediction of heat transfer, a boundary layer with three cells (0.1 mm thickness) was placed on piston, liner and cylinder head boundaries. Simulations were carried out with the same spray setup used for constant-volume calculations, and the temperature wall-functions from Angelberger [1] were used to model heat transfer. Mesh motion was performed using the dynamic mesh layering technique [16], keeping the cells in the spray region fixed and moving the ones in the piston bowl.

Simulations start ad IVC, initial in-cylinder thermo-dynamic conditions were derived from measured data of air flow rate, in-cylinder pressure and air-fuel ratio. Velocity was initialized accounting for instantaneous piston velocity u_p (linearly varying from zero at the head to u_p in the bowl) and swirl ratio, with a wheel flow velocity profile assumed along the cylinder radius. The number of flamelets used depends on the amount of injected fuel mass, for this reason operating point 1 employs 30 flamelets, while for the other two conditions 20 flamelets are adopted for the main injection event and one for the pilot. Such setup does not differ too much from the one used for simulations at constant-volume conditions. Again, new flamelets belonging to the same injection event are initialized with the species and temperature profiles of the previous one. Fig. 9(a) compares computed and experimental data of in-cylinder pressure profiles for the three different operating conditions. For what concerns the full-load case, it is possible to see that experimental pressure profile is rather well

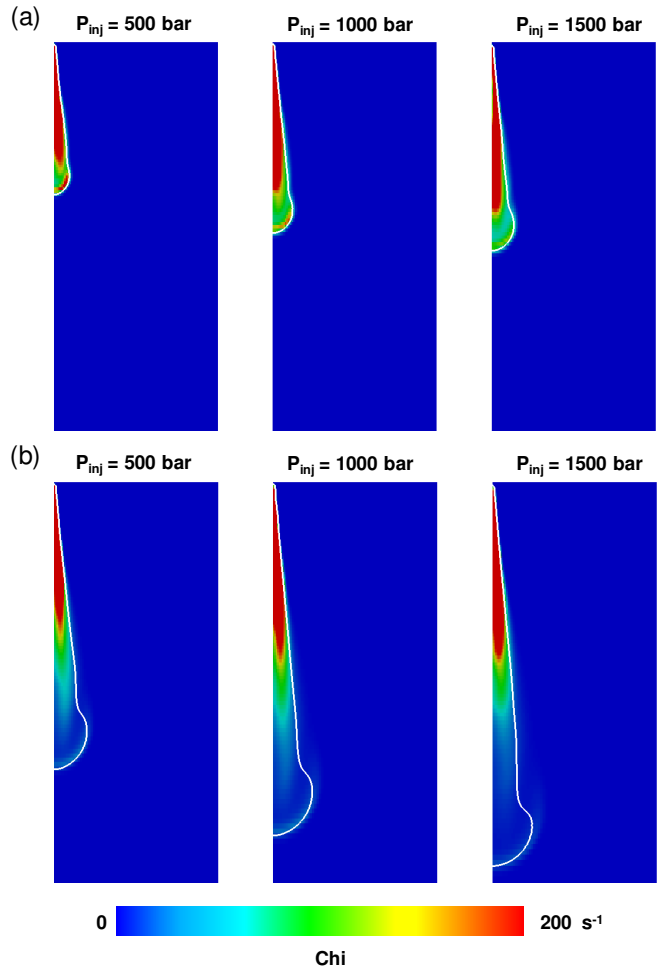

Figure 7: (a): Distribution of the scalar dissipation rate at 0.2 ms ASOI for the cases SA2, SA3 and SA4; (b): Distribution of the scalar dissipation rate at 0.6 ms ASOI for the cases SA2, SA3 and SA4. Scalar dissipation rate range: 0 (blue) - 200 (red).

reproduced by the model. However, peak cylinder pressure is slightly overestimated, and this is mainly affected by the heat release rate (HRR) profile, which is shown in Fig. 9(b). After ignition, in fact, the *mRIF* model predicts a higher combustion speed and this aspect seems to be mainly affected by the mesh resolution used, which is too coarse close to the nozzle. Hence, the predicted scalar dissipation rate remains always well below the extinction limit with a consequent overestimation of the HRR, since flame propagation will also take place close to the nozzle. Heat release rate reaches a maximum around TDC, then it remains constant for approximately 10 CAD. During such period, a diffusion flame structure is fully established, and combustion is both influenced by spray dynamics and flame-wall interaction.

To clarify how flame wall-interaction affects the combustion process, flame

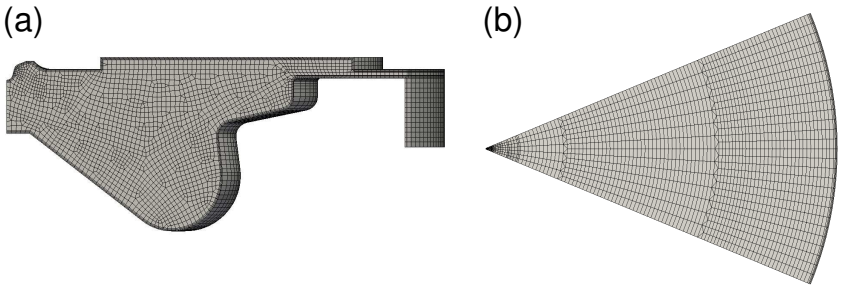

Figure 8: Computational mesh used for combustion simulations of the heavy-duty engine. (a): side view; (b): top view.

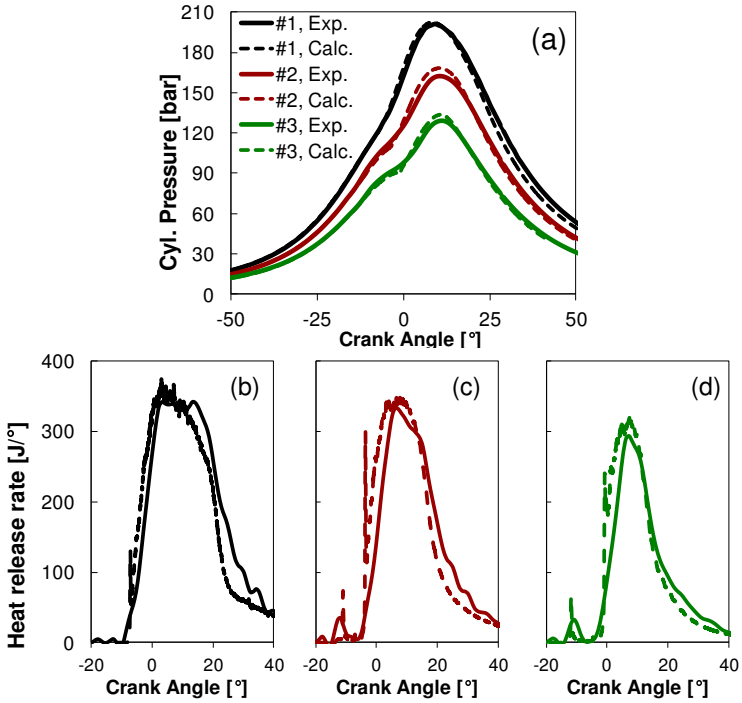

Figure 9: Validation of the *mRIF* model for Heavy Duty Engine simulations: (a) Comparison between computed and experimental pressure traces for operating points 1, 2 and 3; Comparison between computed and experimental heat release rate profiles for operating points 1 (b), 2 (c), 3 (d).

structure was post-processed in terms of temperature field, scalar dissipation rate distribution and its evolution versus time for several flamelets. First of all, it is possible to see that numerically flame and wall starts interacting around 2 CAD BTDC, as it can be seen in Fig. 10(a). This involves the first flamelet and Fig. 10(d) illustrates that, such phenomenon keeps its stoichiometric scalar dissipation rate higher than the next ones. Looking at evolution of the scalar

dissipation rate during injection, Figs. 10(a)-(b), it is possible to see that χ is very high (> 100) in the core of the jet where the mixture is rich, then χ decreases along the jet axis. However, interaction between flame and wall has the beneficial effect of increasing the scalar dissipation rate, allowing to better oxidize the rich combustion products which were generated in the core of the jet. Flame-wall interaction seems to mainly influence combustion for the first flamelets where the piston is very close to TDC. For the remainder of the flamelets, flame-wall interaction does not seem to play a big role because both in-cylinder charge motion and turbulence decay to not affect the scalar dissipation rate which is continuously decreasing. When looking at heat release rate profile, it is possible to see that simulations predicts a earlier decay of combustion speed around 15 CAD, while experimental HRR remains constant for 5 CAD more. Such discrepancy seems, again, to be mainly related to the mesh structure which is not completely spray-oriented. For this reason, numerical diffusion will enlarge the spray region and reduce the jet velocity at the tip with a negative effect of the predicted scalar dissipation rate at the walls. For what concerns the other two operating points, at 75% and 50% load, agreement is acceptable even if there is a slight overestimation of the maximum cylinder pressure due to the overestimated heat release rate after auto-ignition. For both the cases, flame-wall interaction does not seem to play a big role mainly due to the reduced amount which is injected compared to the full-load case.

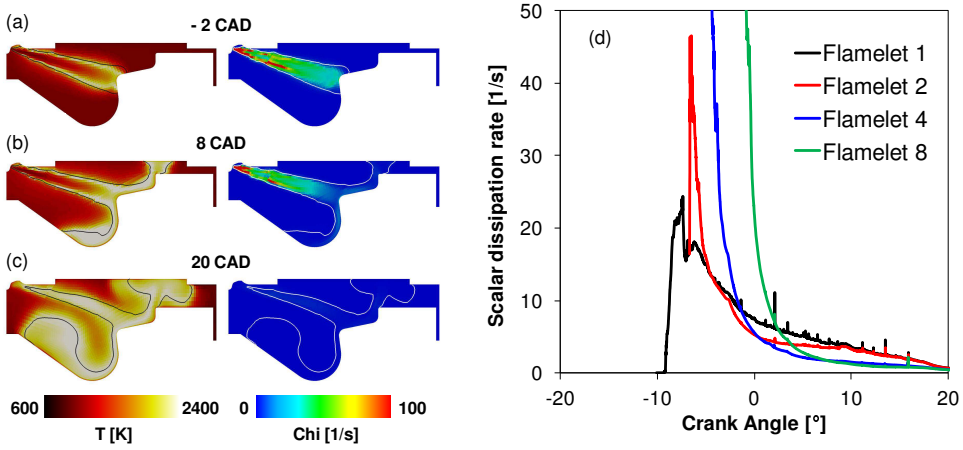

Figure 10: Flame structure analysis of the combustion process for the Heavy Duty Diesel engine: (a) Temperature and scalar dissipation rate distributions at -2, 8 and 20 CAD TDC; (b) evolution of the stoichiometric scalar dissipation rates for flamelets 1, 2, 4 and 8.

5 Conclusions

This work was focused on the development of a CFD methodology for the prediction of the combustion process in Heavy Duty diesel engines. To this end, the *mRIF* (multiple Representative Interactive Flamelets) was implemented into

the Lib-ICE code and applied to both constant-volume and engine simulations. Several techniques were then integrated in order to speed up the CPU time in integrating chemistry and the β-pdf of the chemical species to compute composition in the CFD domain. Satisfactory results were achieved, since the model is able to properly reproduce experimental trends of both ignition delay and flame lift-off for the different conditions, including variation of injection pressure which is quite important for operation of Diesel engines. However, it is necessary to correctly predict the distribution of the scalar dissipation rate, mainly close to the nozzle region, in order to predict the stabilization of the flame. In order to do this, a very fine and spray-oriented mesh seems to be absolutely necessary to describe the mixture fraction and its variance field. Once the proposed approach was validated at constant-volume conditions, engine simulations were carried out in a Heavy Duty engine for three different operating points of interest: full, 75% and 50% load. Despite results can be considered satisfactory, results are affected by mesh resolution and structure which produces an underestimation of the scalar dissipation rate and, consequently, influences heat release rate close to the nozzle and flame wall-interaction process. For this reason, most of the future efforts will be dedicated at improving engine grid generation process to be able to better reproduce both liquid and vapor jet dynamics.

6 List of symbols

6.1 Latin characters

$\mathbf{A}$; mapping gradient matrix;

c_p: specific heat at constant pressure;

C_χ: model constant (2.0);

h: total enthalpy;

h_s: sensible enthalpy;

k: turbulent kinetic energy;

M: flamelet marker;

N_c, N_f, N_s, N_z, N_v: number of cells of the computational domain, number of flamelets, number of chemical species and

P: presumed probability density function (β-PDF);

$\dot{q_s}$: sensible enthalpy source term due to chemical reactions;

$\mathbf{R}$: reaction mapping;

$Sc_Z, Sc_{\widetilde{Z''^2}}$: Schmidt numbers for mixture fraction and its variance;

$\mathbf{U}$: velocity;

Y: chemical species mass fraction;

Z: mixture fraction;

$\widetilde{Z''^2}$: mixture fraction variance; number of points in mixture fraction space, number of virtual species;

6.2 Greek characters

ε: turbulent kinetic energy dissipation rate;

ε_{ISAT}: tolerance of the ISAT method;

μ_t: turbulent viscosity;

ρ: density;

$\sigma_C, \sigma_H, \sigma_O, \sigma_N$: number of carbon, hydrogen, oxygen and nitrogen atoms;

ϕ: equivalence ratio

χ: scalar dissipation rate;

χ_{st}: scalar dissipation rate at stoichiometric mixture fraction;

$\widehat{\chi_{st}}$: conditionally averaged scalar dissipation rate at stoichiometric mixture fraction;

ψ^q; array of compositions (species, temperature, pressure);

$\dot{\omega}_i$: chemical species mass fraction reaction rate;

6.3 Subscripts

χ: referred to scalar dissipation rate;

i, j: referred to chemical species or flamelet;

k: referred to virtual species;

References

[1] Angelberger, C., Poinsot, T., and Delhay, B. Improving Near-Wall Combustion and Wall Heat Transfer Modeling in SI Engine Computations. *SAE Paper 972881* (1997).

[2] Barths, H., Hasse, C., and Peters, N. Computational fluid dynamics modelling of non-premixed combustion in direct injection diesel engines. *International Journal of Engine Research 1 (3)* (2000), pp. 249–267.

[3] Contino, F., Jeanmart, H., Lucchini, T., and DErrico, G. Coupling of in situ adaptive tabulation and dynamic adaptive chemistry: An effective method for solving combustion in engine simulations . *Proceedings of the Combustion Institute Vol. 33(2)* (2011), pp. 3057–3064.

[4] Dec, J. E. A Conceptual Model of DI Diesel Combustion Based on Laser-Sheet Imaging. *SAE Paper 970873* (1997).

[5] D'Errico, G., Lucchini, T., Contino, F., Jangi, M., and Bai, X.-S. Comparison of well-mixed and multiple representative interactive flamelet approaches for diesel spray combustion modelling. *Combustion Theory and Modelling 18*, 1 (2014), 65–88.

[6] D'Errico, G., Lucchini, T., Stagni, A., Frassoldati, A., Faravelli, T., and Ranzi, E. Reduced Kinetic Mechanisms for Diesel Spray Combustion Simulations. *SAE Paper 2013-24-0014* (2013).

[7] Diwakar, R., and Singh, S. NOx and Soot Reduction in Diesel Engine PCCI Combustion: A Computational Investigation. *International Journal of Engine Research 9(3)* (2008), pp. 195–214.

[8] Ferrarese, A., Dias, M., Bruno, R. A., Rejowski, E., and Praca, M. PCU Solutions to Heavy Duty Diesel Engines after Proconve P7. *SAE Paper 2012-36-0358* (2012).

[9] Golovichev, V., Nordin, N., Jarnicki, R., and Chomiak, J. 3-D Diesel Spray Simulations Using a New Detailed Chemistry Turbulent Combustion Model. *SAE Paper 2000-01-1891* (2000).

[10] Idicheria, C. A., and Pickett, L. M. Quantitative Mixing Measurements in a Vaporizing Diesel Spray by Raileigh Imaging. *SAE Paper 2007-01-0647* (2007).

[11] Knecht, W. Strategies for Future Heavy Duty Diesel Engines for Commercial Vehicles. *International Journal of Vehicle Design 14* (2006), pp.67–82.

[12] Lehtiniemi, H., Zhang, Y., Rawat, R., and Mauss, F. Efficient 3-D CFD Combustion Modeling with Transient Flamelet Models. *SAE Paper 2008-01-0957* (2008).

[13] Liang, L., Stevens, J. G., Raman, S., and Farrell, J. T. The use of dynamic adaptive chemistry in combustion simulation of gasoline surrogate fuels. *Combustion and Flame 156*, 7 (2009), 1493 – 1502.

[14] Liu, S., Hewson, J. C., Chen, J. H., and Pitsch, H. Effects of strain rate on high-pressure nonpremixed n-heptane autoignition in counterflow. *Combustion and Flame Vol. 137* (2004), pp. 320–339.

[15] Lucchini, T., D'Errico, G., and Ettorre, D. Numerical investigation of the spraymeshturbulence interactions for high-pressure, evaporating sprays at engine conditions. *International Journal of Heat and Fluid Flow 32*, 1 (2011), 285 – 297.

[16] Lucchini, T., D'Errico, G., Jasak, H., and Tukovic, Z. Automatic Mesh Motion with Topological Changes for Engine Simulation. *SAE Paper 2007-01-0170* (2007).

[17] Lucchini, T., D'Errico, G., Onorati, A., Bonandrini, G., Venturoli, L., and Gioia, R. D. Development of a CFD Approach to Model Fuel-Air Mixing in Gasoline Direct-Injection Engines. *SAE Paper 2012-01-0146* (2012).

[18] Meijer, M., Somers, B., Johnson, J., Naber, J., Lee, S.-Y., Malbec, L. M., Bruneaux, G., Pickett, L. M., Bardi, M., Payri, R., and Bazyn, T. Engine combustion network (ecn): Characterization and comparison of boundary conditions for different combustion vessels. *Atomization and Sprays 22*, 9 (2012), 777–806.

[19] Montenegro, G., Torre, A. D., Onorati, A., Broggi, D., Schlager, G., and Benatzky, C. CFD Simulation of a Sliding Vane Expander Operating Inside a Small Scale ORC for Low Temperature Waste Heat Recovery. *SAE Paper 2014-01-0645* (2014).

[20] Patel, A., Kong, S. C., and Reitz, R. D. Development and Validation of a Reduced Reaction Mechanism for HCCI Engine Simulations. *SAE Paper 2004-01-0558* (2004).

[21] Peters, N. Laminar diffusion flamelet models in non-premixed turbulent combustion. *Progress in Energy and Combustion Science 10* (1984), 319–339.

[22] Pickett, L. M., Genzale, C. L., Bruneaux, G., L.-M. Malbec, L.-M., Hermant, L., Christiansen, C., and Schramm, J. Comparison of diesel spray combustion in different high-temperature, high-pressure facilities. *SAE International Journal of Engines 3*, 2 (2010), 156–181.

[23] Reitz, R. D. Modeling Atomization Processes In High Pressure Vaporizing Sprays. *Atomization and Spray Technology Vol. 3* (1987), pp. 309–337.

[24] Senecal, P. K., Pomraning, E., and Richards, K. J. Multidimensional Modelling of Direct-Injection Diesel Spray Liquid Length and Flame Lift-off Length using CFD and Parallel Detailed Chemistry. *SAE Paper 2003-01-1043* (2003).

[25] Singer, M., and Pope, S. Exploiting ISAT to solve the equations of reacting flow. *Combustion Theory and Modelling Vol. 8* (2004), pp. 361–383.

[26] Som, S., Longman, D., Luo, Z., Plomer, M., and Lu, T. Three Dimensional simulations of diesel sprays using n-dodecane as a surrogate. In *Eastern States Section of the Combustion Institute Fall Technical Meeting* (2011).

[27] Wright, Y. M., Boulouchos, K., Paola, G. D., and Mastorakos, E. Multi-dimensional Conditional Moment Closure Modelling Applied to a Heavy-duty Common-rail Diesel Engine. *SAE Paper 2009-01-0717* (2009).